Correlation between density and temperature fluctuations of hypersonic turbulent boundary layers at $Ma_\infty = 8$

Cite as: AIP Advances **10**, 075101 (2020); https://doi.org/10.1063/5.0013299
Submitted: 11 May 2020 . Accepted: 16 June 2020 . Published Online: 01 July 2020

Xin Li (李欣), Fu-Lin Tong (童福林), Chang-Ping Yu (于长平), and Xin-Liang Li (李新亮)

Correlation between density and temperature fluctuations of hypersonic turbulent boundary layers at $Ma_\infty = 8$

Cite as: AIP Advances 10, 075101 (2020); doi: 10.1063/5.0013299
Submitted: 11 May 2020 • Accepted: 16 June 2020 •
Published Online: 1 July 2020

Xin Li (李欣),[1,2] Fu-Lin Tong (童福林),[1,3] Chang-Ping Yu (于长平),[1] and Xin-Liang Li (李新亮)[1,2,a)]

AFFILIATIONS

[1] LHD, Institute of Mechanics, Chinese Academy of Sciences, Beijing 100190, China
[2] School of Engineering Science, University of Chinese Academy of Sciences, Beijing 100049, China
[3] Computational Aerodynamics Institute of China Aerodynamics Research and Development Center, Mianyang 621000, China

[a)] **Author to whom correspondence should be addressed:** lixl@imech.ac.cn

ABSTRACT

The correlation between density and temperature fluctuations (ρ' and T') of the turbulent boundary layer is significantly affected by wall temperature. Direct numerical simulation databases with the ratio of wall-to-recovery temperature T_w/T_r = 0.8 and 0.15 are considered. A fitting slope method and a two-dimensional correlation method are adopted to visualize the correlated behavior. The results show that an adverse trend and a separated correlated structure are found in the buffer region, which can be treated as the effects of the correlation of ρ' and T'. To reveal the correlation, several statistical analyses are conducted. It indicates that the extreme events in the flow are suppressed with wall cooling; meanwhile, the small-scale fluctuations are enhanced. The behavior of the fluctuations results from the reduced mean swirling strength and the increased radius of the vortical structures.

A turbulent boundary layer (TBL) is a common flow on both supersonic and hypersonic aircrafts. Owing to heat transfer and radiation, the wall temperature is usually lower than the adiabatic condition. It is necessary to essentially reveal a further physical mechanism of the changed flow features.[1] Thus, the hypersonic TBL with different wall temperatures attracts many researchers' attention. Recently, direct numerical simulation (DNS) becomes an effective method for the compressible flow study.[2–4] Some of the previous studies have considered different wall temperatures. With the ratio of wall-to-recovery temperature, T_w/T_r = 1–0.18, the validity of Morkovin's hypothesis is verified at moderate free-stream Mach numbers.[5] It is found that the compressible effect is enhanced with decreasing wall temperature, but is still weak.[6] Later, the structure of pressure fluctuation[7] and the inclination angle of the vortices are investigated with the effect of wall cooling.[8] However, limited by the numerical method and computational resource, DNS is primarily adopted under relatively low Mach number conditions.[9,10] Few studies provide detailed statistics of hypersonic TBLs. The accurate correlation of density and temperature fluctuations (ρ' and T″) are usually studied to construct TBL's model, and one of the correlation expressions was early driven by Rubesin.[18] Later, their statistical behaviors are further exhibited.[12–14] However, any studies of the correlation of T' and ρ' at high Mach numbers is still scarce.

The objective of the current study is to investigate the statistical behavior of ρ' and T' and their correlation. To begin with, a fitting slope of the correlation of ρ' and T' is obtained. Then, a two-dimensional correlation method is adopted to illustrate the correlated structures. Furthermore, the cause of the change in the correlation is revealed by statistical analyses.

Two DNS datasets presented in previous studies are considered.[15,16] The x, y, and z represent the streamwise, wall-normal, and spanwise directions, respectively. Some flow conditions are summarized in Table I, where Ma_∞ and T_∞ are the free-stream Mach number and temperature, respectively. The thermal boundary conditions for the walls of high and low wall temperature cases (TH and TL, respectively) are isothermal with T_w/T_r = 0.8 and 0.15,

TABLE I. Flow parameters for the DNS database.

Case	Ma_∞	T_∞ (K)	T_w/T_∞	$Re_{\delta 2}$	δ
TH	8	169.44	10.03	6328.23	0.25
TL	8	169.44	1.9	6763.45	0.12

where $T_r \equiv T_\infty[1 + ((\gamma - 1)/2)Ma_\infty^2 r]$, with the turbulent recovery factor $r = 0.89$. $Re_{\delta 2} = \rho_\infty U_\infty \theta/\mu_w$ is defined by the ratio of the highest momentum to the wall shear stress,[17] where θ is the momentum thickness. For the TH and TL cases, the domain sizes ($L_x \times L_y \times L_z$) are $37 \times 0.7 \times 0.3$ and $11 \times 0.7 \times 0.18$, respectively, which are nondimensionalized by inches. The mesh numbers ($N_x \times N_y \times N_z$) are $12\,460 \times 100 \times 320$ and $8950 \times 90 \times 640$, corresponding to the grid sizes ($dx^+ \times dy^+ \times dz^+$), $12.2 \times 0.96 \times 4.6$ and $11.2 \times 1.0 \times 4.5$. The total time of the sampling snapshots of the y–z plane spans is $22\delta/U_\infty$ for TH and $72\delta/U_\infty$ for TL. More details of the computational setup can be found in the previous study.[15]

Using the polytropic assumption, the near-wall behavior of the instantaneous normalized density fluctuation ($\rho'/\bar{\rho}$) and temperature fluctuations ($T'/\bar{T}$) can be predicted by[6]

$$\frac{p'}{\bar{p}} = n\frac{\rho'}{\bar{\rho}} = \frac{n}{n-1}\frac{\rho T'}{\bar{\rho}\bar{T}}. \tag{1}$$

Here, the polytropic coefficient n is treated as a turbulence modeling parameter. For isobaric conditions, $n = 0$.[18] At a supersonic channel flow, it takes $n = 0$ and the slope is -1.[11] In order to illustrate the complete view of the relation across the TBL, the slopes from the present DNS are shown in Fig. 1. The slope at each wall-normal position is calculated by applying the least square method to the scatter plots of $\rho'/\bar{\rho}$ and $\frac{\rho T'}{\bar{\rho}\bar{T}}$. It is shown that the slopes for both cases are close to zero near the wall. Then, they tend to a relatively strong anti-correlation that the slope is equal to -1 as the distance from the wall increases. Unlike expected, an adverse trend toward zero at $y^+ = 28$ is found for TL. The results are different with those of supersonic cases.[6] The rapid changes at $y^+ \approx 2000$ are related to the free-stream flow.

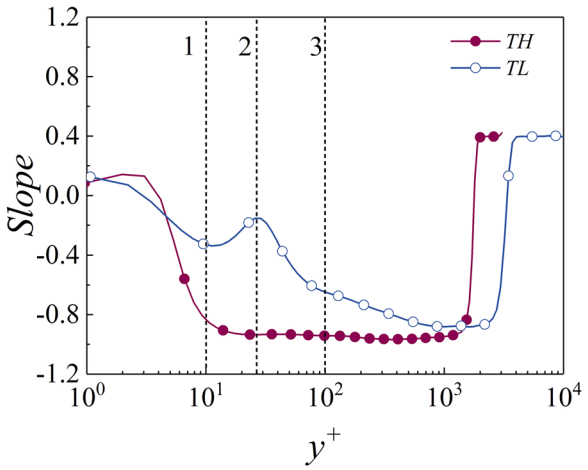

FIG. 1. Slope of the normalized temperature fluctuations as functions of density fluctuations.

Although the right-hand-side also contains ρ, it can still be reasonably inferred that the left-hand-side maybe related to ρ or T'. To reveal this confusion and demonstrate the detailed correlation of ρ' and T', a two-dimensional correlation analysis is performed. The correlation coefficient $R_{\rho' T'}$ is defined by

$$R_{\rho' T'}(y_r; x_s, y_s, z_s) = \frac{\overline{\rho'(x, y_r, z)T'(x + x_s, y_s, z + z_s)}}{\rho'_{rms}(y_r) \cdot T'_{rms}(y)}, \tag{2}$$

where the subscript r denotes a fixed reference point and s represents moving points in the three-dimensional space. This analysis has been used to identify the feature of coherent structures.[19–21] Owing to the aperiodicity in the streamwise direction for flat plate flow, x_s is not considered. $R_{\rho' T'}$ represents the correlation of T' at other points onto ρ' at the reference point. Positive $R_{\rho' T'}$ means a positive contribution from other points to the current position and vice versa.

Considering y_r at three typical wall-normal positions denoted as 1, 2, and 3 shown in Fig. 1, further evidence of the existence of the adverse trend is plotted in Fig. 2. For TH, there is only a negative correlated region around the reference wall-normal distance $y_r = 10.8$ [see Fig. 2(a)]. With the increase in y_r, the negative correlation extends in both wall-normal and spanwise directions [see Figs. 2(b) and 2(c)], which achieves a good agreement with the increased sizes of the lift-up vortices.[22] It demonstrates that the correlation is dominated by the local ρ' and the surrounding negative correlated T' for TH.

For the TL case, it can be found in Fig. 2(d) that a small negative correlation is surrounded by a large range of positive correlations. As shown in Fig. 2(e), the contour of positive correlation breaks into three separated positive correlated regions, in the center of which is a negative correlated region. This reference distance y_r corresponds to the position of the adverse trend shown in Fig. 1. The maximum and minimum, respectively, refer to the surrounding positive correlation and the local negative correlation, which are 20%. It indicates that the surrounding T' takes about 20% positive effect on the local ρ', whose magnitude accords with the adverse trend. As shown in Fig. 2(f), the contour of $R_{\rho' T'}$ consists of a double-layer structure with opposite correlation signs. The lower part is a flattened positive correlation, above which is a negative correlated elliptical region. For TL, it indicates that the correlation results from the local ρ' and the partial surrounding positive correlated T'. As indicated in Fig. 2, the two-dimensional correlation indicates that the adverse trend is very likely coming from ρ' and T' and the correlation between the surrounding T' and the local ρ' is verified.

The correlation of ρ' and T' can be further studied by their occurrences in the TBL. To reveal the cause of the correlation, the probability density functions (P. D. F) of ρ' and T' are computed, as shown in Fig. 3. It is seen that the positive and negative P. D. F. tails are shortened, addressing that the probabilities of the large-scale fluctuations of ρ' and T' decrease. It means that the extreme events are weakened. The results indicate that the correlation of ρ' and T' is dominated by the small-scale fluctuations for the case of a strong cold-wall.

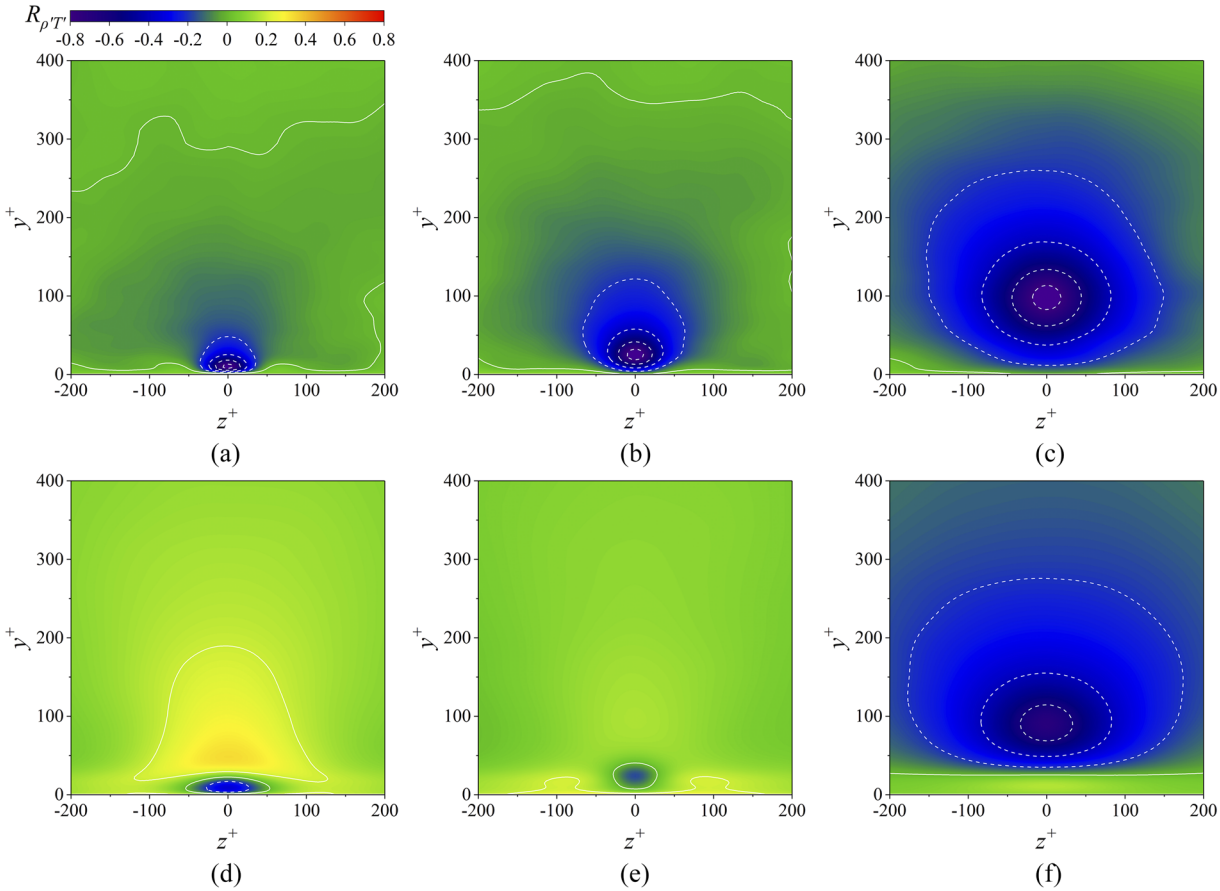

FIG. 2. Correlation $R_{\rho'T'}$ with y_r at three wall-normal locations. The solid white line denotes $R_{\rho'T'} = 0$. [(a)–(c)] y_r = 10.8, 27.9, and 105.1 for TH, respectively. [(d)–(f)] y_r = 9.5, 28.8, and 100.2 for TL, respectively.

The skewness factor (S) is considered to assess the high-order statistical behavior of ρ' and T'. For example, $S(\rho')$ is defined as

$$S(\rho') = \frac{\overline{\rho'^3}}{\overline{\rho'^2}^{3/2}}. \tag{3}$$

The skewness across the TBL is given in Fig. 4. As mentioned in the work of Kim,[23] adequate data points should be considered; otherwise, the skewness is difficult to converge. The results of the present DNS show no oscillation, demonstrating the convergent skewness.

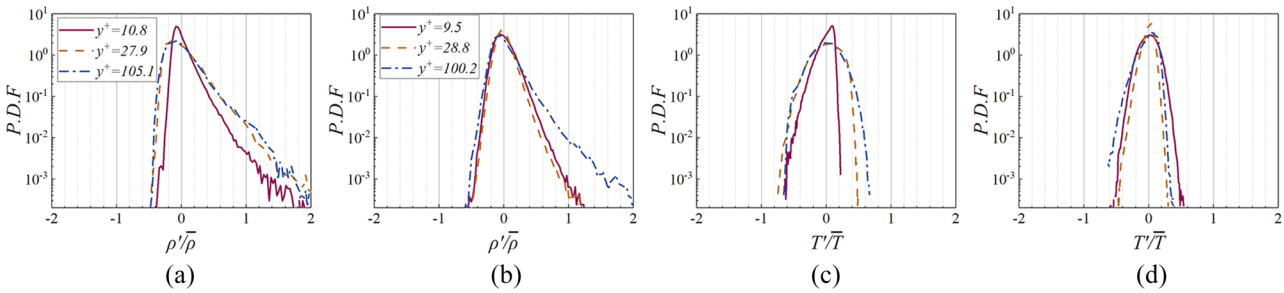

FIG. 3. Probability density function of ρ' and T' normalized by the mean values at the three typical wall-normal positions. [(a) and (c)] P. D. F of ρ' and T' for TH, respectively. [(b) and (d)] P. D. F of ρ' and T' for TL, respectively.

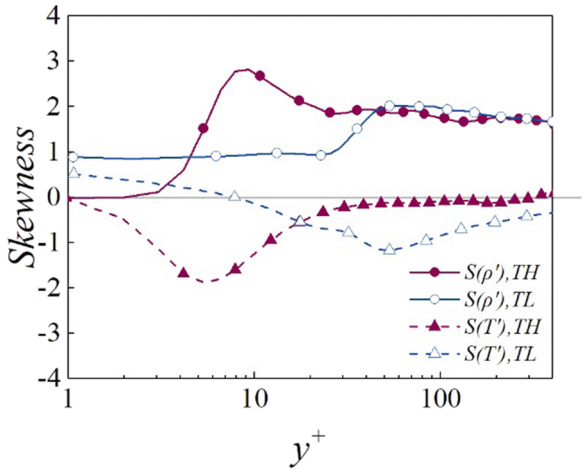

FIG. 4. Skewness of ρ' and T' for TH and TL.

The profiles are approximately symmetrical about the axis of $S = 0$, which supports most of the anti-correlation of ρ' and T' far from the wall. Note the similarity in the trend of current results with those from the work of Wei.[24] By cooling the wall, the first local maximum as $S(\rho') = 3$ decreases to $S(\rho') = 2$ as well as the corresponding wall-normal position at $y^+ = 10$ increases to $y^+ = 50$. $S(T') = 2$ decreases to $S(T') = 1.2$ with $y^+ = 6$ increasing to $y^+ = 50$. It supports the fact that the large-scale fluctuations of ρ' and T' are reduced by wall cooling. Meanwhile, the small-scale ones are enhanced, which causes the correlation through the spatial distance. It is also inferred that more organizational vortices are produced in the cooled-wall case.

According to previous analyses, one of the main reasons for the correlation is due to the relatively organizational vortical structures produced in TL. Thus, to investigate the geometrical features of vortical structures, some statistics relating to the coherent structures are performed.

Figure 5 provides the P. D. F. of $(u'\omega'_x)^+$ whose isosurface is always used to represent the profile of the statistical coherent structures,[25] and the probability density can help us have some insight into the change in the vortices. It can be observed that the large-scale fluctuations decrease when cooling the wall, especially at the two locations near the wall. However, the line at $y^+ = 28.8$ is higher than the others for TL, which indicates an inverse trend being consistent with the correlation of ρ' and T', as shown in Fig. 2(e). It is inferred that the geometrical feature and the movement of the vortical structures are the possible physical origin of the inverse trend.

Thus, in attempting to support this view, the statistical curvature of vortex lines is considered. The instantaneous vortex line is going to be always tangent to the vorticity. The local radius of curvature of a vortex line R is defined as[26]

$$R = \frac{\omega^3}{|\boldsymbol{\omega} \times (\nabla \boldsymbol{\omega} \cdot \boldsymbol{\omega})|}, \tag{4}$$

where $\boldsymbol{\omega}$ in the denominator is a local vorticity vector and ω in the numerator is the mode of $\boldsymbol{\omega}$. R is normalized by one wall unit. Figure 6 depicts the distribution of R^+. It is observed that R^+ varies

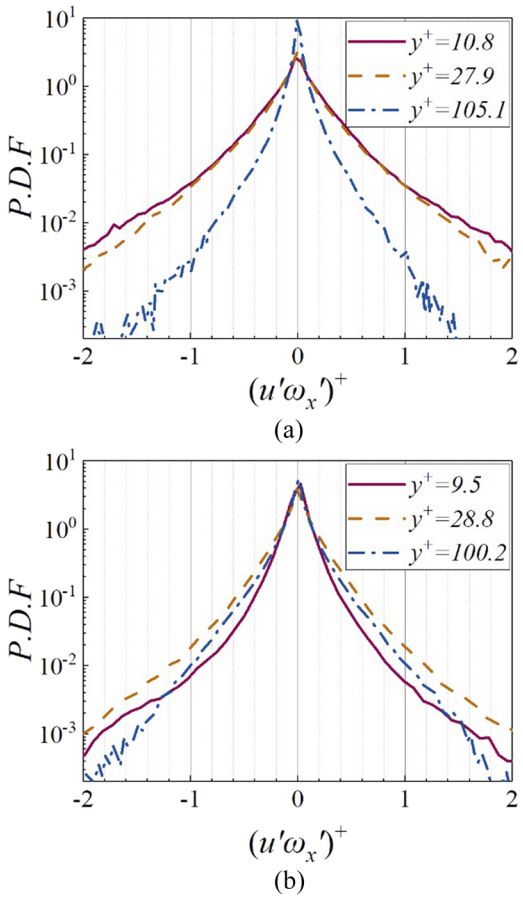

FIG. 5. Probability density function of the normalized $(u'\omega'_x)^+$ at the three typical wall-normal positions. (a) TH and (b) TL.

between 40 and 80 wall units except for the extreme near-wall region for TH, which collapses the result at relatively low free-stream Mach numbers.[10] With the decrease in the wall temperature, it is seen that R^+ significantly increases about three times than the TH case, indicating that the vortical structures become larger.[14]

To further verify the decrease in the extreme events, the swirling strength λ_{ci} is computed. As shown by Zhou[27] and Stanislas,[28] λ_{ci} is the imaginary part of the complex eigenvalue of the velocity gradient tensor. Figure 7 plots λ_{ci} in the swirling region ($\Delta > 0$), where Δ is a discriminant of the velocity gradient tensor, given as

$$\Delta = \frac{27}{4}R^2 + \left(P^3 - \frac{9}{2}PQ\right)R + \left(Q^3 - \frac{1}{4}P^2Q^2\right). \tag{5}$$

It is observed that a strong swirling activity occurs in the near-wall region for both cases and then decays with the distance from the wall. The maximum of the swirling strength decreases with wall cooling. The position of the maximum value for TL is farther than that of TH, corresponding to the increased wall-normal position of the turbulent kinetic production term and the increased spanwise spacing of the near-wall streaks.[29] The decreased maximum of λ_{ci}

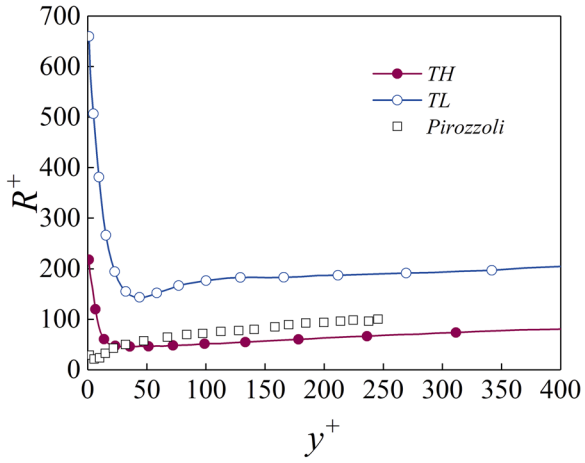

FIG. 6. Mean radius of curvature of the vorticity field for TH and TL.

demonstrates that the extreme events are suppressed by cold wall temperature.

In summary, the correlation between ρ' and T' is investigated on two flat-plate DNS datasets with high and low wall temperatures. The fitting slopes, two-dimensional correlation, and the statistics related to the vortical structures are performed.

The present results show that the adverse trend of the slope occurs in the buffer region under cooled-wall conditions. The contribution of the surrounding-to-local correlation is about 20%, which is shown by the contour of the two-dimensional for TL. The statistical analyses show that the surrounding-to-local correlation results from the decreased extreme events and the enhanced small-scale fluctuations with the cold wall temperature. Furthermore, it is found that these changes in the fluctuations of ρ' and T' are caused by the increased radius of the vortices, which is conducive to the spatial transport of the small-scale fluctuations. Later, it is supported that the relatively weak swirling strength results in the decreased

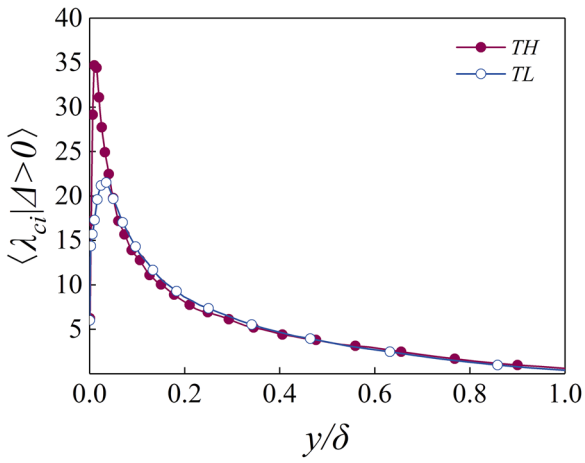

FIG. 7. Wall-normal evolution of conditional mean swirling strength λ_{ci}^+.

extreme events. This work gives further insight into the statistical behavior under the hypersonic condition.

This work was supported by the National Numerical Wind Tunnel Project, the National Key Research and Development Program of China (Grant Nos. 2019YFA0405300 and 2016YFA0401200), NSFC Projects (Grant No. 91852203), the Science Challenge Project (Grant No. TZ2016001), and the Strategic Priority Research Program of Chinese Academy of Sciences (Grant No. XDC01000000). The authors would like to thank the National Supercomputer Center in Tianjin (NSCC-TJ) and National Supercomputer Center in Guangzhou (NSCC-GZ) for providing computer time.

DATA AVAILABILITY

The data that support the findings of this study are available from the corresponding author upon reasonable request.

REFERENCES

[1]X. K. Zhu, C. P. Yu, F. L. Tong, and X. L. Li, "Numerical study on wall temperature effects on shock wave/turbulent boundary-layer interaction," AIAA J. **55**(1), 131–140 (2016).
[2]M. Lagha, J. Kim, J. D. Eldredge, and X. L. Zhong, "Near-wall dynamics of compressible boundary layers," Phys. Fluids **23**, 065109 (2011).
[3]M. Lagha, J. Kim, J. D. Eldredge, and X. L. Zhong, "A numerical study of compressible turbulent boundary layers," Phys. Fluids **23**, 015106 (2011).
[4]L. Duan, I. Beekman, and M. P. Martín, "Direct numerical simulation of hypersonic turbulent boundary layers. Part 3. Effect of Mach number," J. Fluid Mech. **672**, 245–267 (2011).
[5]L. Duan, I. Beekman, and M. P. Martín, "Direct numerical simulation of hypersonic turbulent boundary layers. Part 2. Effect of wall temperature," J. Fluid Mech. **655**, 419–445 (2010).
[6]M. S. Shadloo, A. Hadjadj, and F. Hussain, "Statistical behavior of supersonic turbulent boundary layers with heat transfer at $M_\infty = 2$," Int. J. Heat Fluid Flow **53**, 113–134 (2015).
[7]C. Zhang, L. Duan, and M. M. Choudhari, "Effect of wall cooling on boundary layer-induced pressure fluctuations at Mach 6," J. Fluid Mech. **822**, 5–30 (2017).
[8]S. Sharma, M. S. Shadloo, and A. Hadjadj, "Turbulent flow topology in supersonic boundary layer with wall heat transfer," Int. J. Heat Fluid Flow **78**, 108430 (2019).
[9]S. Pirozzoli, M. Bernardini, and F. Grasso, "Characterization of coherent vortical structures in a supersonic turbulent boundary layer," J. Fluid Mech. **613**, 205–231 (2008).
[10]S. Pirozzoli, "On the size of the eddies in the outer turbulent wall layer: Evidence from velocity spectra," in *Progress in Wall Turbulence 2* (Springer, Cham, 2016), pp. 3–15.
[11]M. W. Rubesin, "Extra compressibility terms for Favre-average two equation model of inhomogeneous turbulent flow," Technical Report No. 177556, NACA CR, 1990.
[12]G. N. Coleman, J. Kim, and R. D. Moser, "A numerical study of turbulent supersonic isothermal-wall channel flow," J. Fluid Mech. **305**, 159–183 (1995).
[13]M. P. Martin, "Direct numerical simulation of hypersonic turbulent boundary layers. Part 1. Initialization and comparison with experiments," J. Fluid Mech. **570**, 347–364 (2007).
[14]Y.-B. Chu, Y.-Q. Zhuang, and X.-Y. Lu, "Effect of wall temperature on hypersonic turbulent boundary layer," J. Turbul. **14**, 37–57 (2013).
[15]X. Liang and X. L. Li, "Direct numerical simulation on Mach number and wall temperature effects in the turbulent flows of flat-plate boundary layer," Commun. Comput. Phys. **17**, 189–212 (2015).
[16]X. Li, F. L. Tong, C. P. Yu, and X. L. Li, "Statistical analysis of temperature distribution on vortex surfaces in hypersonic turbulent boundary layer," Phys. Fluids **31**(10), 106101 (2019).

[17]H. H. Fernholz and P. J. Finley, "A critical commentary on mean flow data for two-dimensional compressible boundary layers," AGARD-AG-253, 1980.
[18]M. W. Rubesin, "A one-equation model of turbulence for use with the compressible Navier-Stokes equations," NASA Report No. TM X-73, 1976.
[19]M. J. Ringuette, M. Wu, and M. P. Martín, "Coherent structures in direct numerical simulation of turbulent boundary layers at Mach 3," J. Fluid Mech. **594**, 59–69 (2008).
[20]J. Pei, J. Chen, H. Fazle, and Z.-S. She, "New scaling for compressible wall turbulence," Sci. China: Phys., Mech. Astron. **56**(9), 1770–1781 (2013).
[21]J. Chen, F. Hussain, J. Pei, and Z.-S. She, "Velocity–vorticity correlation structure in turbulent channel flow," J. Fluid Mech. **742**, 291–307 (2014).
[22]X. Wu and P. Moin, "Direct numerical simulation of turbulence in a nominally zero-pressure-gradient flat-plate boundary layer," J. Fluid Mech. **630**, 5–41 (2009).
[23]J. Kim, P. Moin, and R. Moser, "Turbulence statistics in fully developed channel flow at low Reynolds number," J. Fluid Mech. **177**, 133–166 (1987).
[24]L. Wei and A. Pollard, "Direct numerical simulation of compressible turbulent channel flows using the discontinuous Galerkin method," Comput. Fluids **47**(1), 85–100 (2011).
[25]J. Pei, J. Chen, Z. S. She, and F. Hussain, "Model for propagation speed in turbulent channel flows," Phys. Rev. E **86**(4), 046307 (2012).
[26]G. Farin, *Curves and Surfaces for Computer-Aided Geometric Design: A Practical Guide* (Elsevier, 2014).
[27]J. Zhou, R. J. Adrian, S. Balachandar, and T. M. Kendall, "Mechanisms for generating coherent packets of hairpin vortices in channel flow," J. Fluid Mech. **387**, 353–396 (1999).
[28]M. Stanislas, L. Perret, and J.-M. Foucaut, "Vortical structures in the turbulent boundary layer: A possible route to a universal representation," J. Fluid Mech. **602**, 327–382 (2008).
[29]X. Liang and X. L. Li, "DNS of a spatially evolving hypersonic turbulent boundary layer at Mach 8," Sci. China: Phys., Mech. Astron. **56**(7), 1408–1418 (2013).